Inorganic Chemistry

Article

pubs.acs.org/IC

Site Preference and Ordering Induced by Au Substitution in the γ-Brass Related Complex Au−Cr−Zn Phases

Partha P. Jana,*[,†,‡] Ryan Henderson,[§] Bernd Harbrecht,[‡] and Sven Lidin[†]

[†]CAS Chemical Centre, Lund University, Getingevägen 60, Box 124, SE-22100, Lund, Sweden

[‡]Department of Chemistry and Center for Material Sciences, Philipps University Marburg, Hans-Meerwein-Strasse, D-35032, Marburg, Germany

[§]Department of Chemistry and Chemical Biology, Cornell University, Ithaca, New York 14853-1301, United States

Supporting Information

ABSTRACT: The crystal chemistry of the ternary Au−Cr−Zn alloy was studied by means of synthesis, single crystal X-ray diffraction, and electron structure calculations. While the compound $CrZn_{\sim 17}$ represents the binary end-point of the homogeneity range, the inclusion of Au proves to be very site specific, and at the limiting composition $Au_{10}Cr_4Zn_{89}$ the structure is completely ordered. The crystallographic site occupancy pattern calculated by the Local Density Approximation (LDA)-Density Functional Theory (DFT) parametrized extended Hückel (eH) Mulliken charge populations in $Au_{10}Cr_4Zn_{89}$ agrees very well with the experimentally found site occupancy pattern.

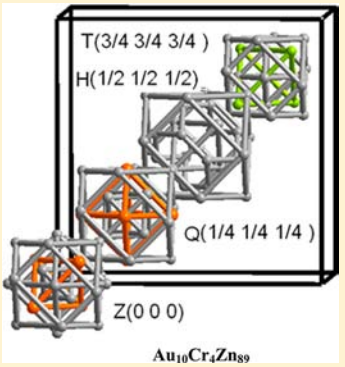

INTRODUCTION

Hume−Rothery phases[1,2] are formed between elements of group 2, 12−14, and transition elements, preferably noble metals. They mostly display medium to large homogeneity ranges. Hume−Rothery phases achieve their stability by the lowering the kinetic energy of the valence electrons associated with a reduction of density of states at the Fermi level. Such reduction is achieved because of the interaction between the Fermi surface of radius k_F and the Brillouin zone characterized by a reciprocal lattice vector.[3,4]

The γ-brass phases are of particular interest among the Hume−Rothery phases because of their structural complexity. The archetypical example of γ-brass is Cu_5Zn_8[5−7] which contains two formula units with a lattice parameter, $a \approx 900$ pm in the body-centered cubic space group $I\bar{4}3m$. The atomic arrangement of γ-brass may be generated by starting from a 3 × 3 × 3 superstructure of a bcc packing of atoms followed by removing two atoms from the resulting 54-atom super cell (one from the vertex, one from the center of the super cell), then relaxing the remaining atomic sites to compensate for the vacancies.[7] By several experimental and theoretical means, it has been shown for γ-brass phases that the ideal *vec* value is 21/13 per atom.

Zn-rich systems appear to be particularly prone to form γ-brass based phases. While there are several recent reports on Zn-based γ-brass type systems with the composition M_2Zn_{11} (M = Ni, Rh, Ir)[8−10] some transition metal−zinc systems accommodate bundles of phases with a bewildering compositional and structural complexity.[11−15] Among these complex crystalline phases, that most closely related to γ-brass is a $2a \times 2a \times 2a$ superstructure.[16,17] Such phases have been reported in several binary systems, such as $Fe_{22}Zn_{78}$,[18] $MoZn_{20.44}$,[19] Pt_5Zn_{21},[20] $Ir_{7+7\delta}Zn_{97-11\delta}$[21] and, most recently, $CrZn_{17-\delta}$.[22] In spite of their structural and compositional differences, these cubic giant cell structures can be uniformly visualized by decomposing them into four symmetrically independent structural units each consisting of 22−29 atom clusters centering around the distinct high symmetry points of the cell, that is, (0 0 0), ($^1/_4$ $^1/_4$ $^1/_4$), ($^1/_2$ $^1/_2$ $^1/_2$), ($^3/_4$ $^3/_4$ $^3/_4$). In standard notation each cluster type is designated by number (1−4), that is, 1 for (0 0 0), 2 for ($^1/_4$ $^1/_4$ $^1/_4$), 3 for ($^1/_2$ $^1/_2$ $^1/_2$), and 4 for ($^3/_4$ $^3/_4$ $^3/_4$). Furthermore, the clusters will be differentiated by a set of three or four atomic shells composing the clusters. Furthermore, we numerate atoms of a given cluster according to their distance from the center of the cluster.

In this paper we report on the ordering occurring on site specific Au substitution in $CrZn_{17}$. We have chosen gold for substitution because of its strong scattering factor compared to that of chromium and zinc. This fact permits distinguishing the atomic sites of gold by the result of X-ray diffraction experiment.

EXPERIMENTAL SECTION

About 15 reactions were carried out with different Au/Cr ratios in $(Au_xCr_{1-x})Zn_{\sim 15}$ starting from the pure elements: Au (99.99%,

Received: October 14, 2012
Published: April 22, 2013

   dx.doi.org/10.1021/ic302244e | Inorg. Chem. 2013, 52, 4812−4818

ABCR), Cr (99.995%, Aldrich), and Zn (99.9999%, Chempur). Samples of precisely weighed metals (ca. 0.3 g each) were loaded and sealed in fused silica ampules (3 cm long, 0.8 cm in diameter) under a reduced argon pressure of about 0.5 Pa. The metals were heated at a rate of 194.4 K h^{-1} up to 1273 K at which the ampules were kept for 2 h. Here after, the temperature was reduced to 703 K at a rate of 114 K h^{-1} and annealed at this temperature for 5 days. Subsequently the samples were either quenched in cold water or cooled to ambient temperature. To avoid loss of zinc because of evaporation, the reaction took place at the cooler end of the ampule. Products obtained from these reactions were silvery, brittle ingots and were found to be stable in air. In a few cases, small amounts of gaseous zinc recondenses into tiny globules in close contact with the regular, brittle, silvery, lustrous metallic products. In some cases crystals have regular shape (Figure 1).

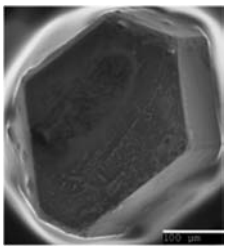

Figure 1. Scanning electron micrograph of a regular form of a crystal of $Au_{4.59}Cr_{4.85}Zn_{91.33}$.

X-ray Diffraction Data Collection and Processing. Eleven single crystals ranging from $0.02 \leq x_{Au} \leq 0.10$ selected from different Au−Cr−Zn reactions were studied by means of X-ray diffraction. Crystallographic details of all the specimens are listed in the Supporting Information. The diffraction intensities were recorded with an imaging plate diffraction system IPDS (Stoe & Cie.) working with MoKα radiation.[23] The patterns could be indexed on the basis of a 1.8 nm large F-centered cubic unit cell. The measured intensities were corrected for Lorentz and polarization effects and for absorption by using the STOE X-RED and X-SHAPE programs.[24,25] For all the specimens, systematic absences and Wilson plots revealed an acentric face-centered cubic crystal system with the Laue Group $m\bar{3}m$. The structures were solved in the acentric space group $F\bar{4}3m$ (No. 216) by applying direct methods and refined using the SHELX-97 program package based on full-matrix least-squares refinements.[26] Additional atomic positions were identified in residual electron density maps. At this stage the structure refinements converged at $R(F) < 0.17$. Further improvement of the model was achieved by partially replacing chromium and/or zinc by gold on the site which showed lower displacement parameters with respect to normal, assuming those sites to be fully occupied by mutual substitution of the two components. On the other hand, those metal sites having relatively large thermal displacement parameters were checked for partial occupancy and positional disorder. Atoms for which the refined occupancy factors deviated by less than twice the standard deviation from unity were reset to unity in the final refinement cycles. Local structural disorder phenomena were modeled by introducing split positions. There are several physically impossibly short distances in the structure. For example d(Zn10−Zn11) and d(Cr20−Zn21) are too short. In no case does the sum of site occupancy factors (SOFs) of two such sites exceed unity, but the splits are explainable in terms of a set of locally ordered clusters. The independently refined SOFs of those adjacent atomic sites show the relations: SOF(Zn10) + SOF(Zn11) = 1 and SOF(Cr20) + SOF(Zn21) = 1.

The site Zn23 site shows a particularly high degree of spatial disorder and must be modeled using two additional sites Zn23′ and Zn23″. Independent refinements of the fractional occupancies for Au-poor samples having composition of $x_{Au} = 0.026, 0.027, 0.032$ result in the relation: SOF(Zn23) + 2 SOF(Zn23′) + 2 SOF(Zn23″) ≈ 1. Correspondingly, the Au-rich sample of $x_{Au} = 0.077$ confirms the relation SOF(Au23) + 2 SOF(Zn23′) + 2 SOF(Zn23″) ≈ 1 and for the sample $x_{Au} = 0.097$, SOF(Au23) = 1. For the crystals of nominal composition ranging from $0.077 > x_{Au} \geq 0.038$, the sum of SOFs of the three sites (Zn23, Zn23′, and Zn23″) shows considerable deviations from full occupancy. This problem can be resolved if we assume that mutual statistical substitution of two constituents (Au and Zn) on Zn23 sites obey the previous relation. All the disordered sites were refined with noncoupled occupation parameters except the ones showing mixed occupancy. Each structure was checked for possible twinning by inversion and its absolute configuration by making use of a possible violation of Friedel's law due to the anomalous dispersion effect. The anisotropic displacement parameters of all the atoms except a few positional disordered sites were refined. The final refinement including an extinction correction and a proper weighting scheme yields $R(F)$ values between 0.032 and 0.054. Details of the crystal structure investigations can be obtained from the Supporting Information.

All the samples were examined by X-ray powder diffractometry to check the purity of single-phase samples, to determine the adjacent phases, and to identify new phases. The powder diffraction data were collected by a X′ Pert MPD diffractometer (CuKα = 1.5406 Å, 40 kV, 40 mA) made by Philips operating in Bragg−Brentano geometry using a secondary monochromator (Graphite). The powders were evenly distributed in a single crystal silicon plate. All the diffractograms were recorded between $5° < 2\theta < 90°$ at room temperature.

Energy Dispersive X-ray Analyses and Scanning Electron Microscopy. A scanning electron microscope (CS-4DV, CAM Scan 20 kV) equipped with an EDS (Energy Dispersive X-ray Spectroscopy) with SiLi detector (Thermo Noran Instruments, Pt-L, Zn-L) was used to obtain a pictorial representation of the studied objects and to determine the approximate elemental composition of a sample. The analysis was carried out with the Voyager program from Thermo Noran. EDS spectra were recorded from those samples which had been previously studied by single crystal X-ray diffraction experiments. No impurities of elements heavier than carbon were detected to be present in the selected specimens.

Thermal Analysis. Thermo-chemical analyses were performed by employing a differential scanning calorimeter operating in the temperature range 300−1273 K (DSC setsys 16/18 Setaram, Pt/Rh thermocouple). 30−40 mg samples were pressed to pellets of 0.3 cm in diameter and then placed into small silica ampules of external diameter of 0.5 cm. The silica ampules were sealed under a reduced pressure. The length of the sample container was reduced to ≈1.5 cm to suppress incongruent vaporization of Zn. An empty silica container of similar size was used as a reference. The experiments were carried out under argon atmosphere at constant pressure. To ensure reproducibility of the thermal events the experiments were repeated twice at heating and cooling rates of 10 K min^{-1}.

Computational Details. Density of states (DOS) plots for $Au_{10}Cr_4Zn_{89}$ were generated with VASP[27−30] using the Local Density Approximation (LDA)[31] and ultrasoft pseudopotentials.[32,33] There are 103 ions in the primitive cell, and we used 35 k-points in the irreducible wedge of the Brillouin zone. The energy cutoff was 250 eV.

The extended Hückel (eH) calculations were performed using YAeHMOP. In the eH calculation, one needs to choose values for diagonal elements of the Hamiltonian, H_{ii}, and the Slater exponents, ζ.

To choose these atomic parameters for Zn, we tried to qualitatively match the s- and p- band structure from the eH calculation to that of the LDA-DFT calculation. For this purpose, a separate LDA-DFT Zn calculation was run with 201 k-points (40 k-points between each special k-point) to generate a Zn band structure. The experimental lattice constants for Zn were used without geometry optimization because of well-known difficulties in finding computationally the correct c/a ratio in elemental Zn.[34]

The Zn parameters used for the qualitative fitting (Supporting Information, Figure S3), and on the "all-Zn" $Au_{10}Cr_4Zn_{89}$ calculation, are: H_{ii}(4s) = −8.96 eV, H_{ii}(4p) = −4.36 eV, ζ(4s) = 1.35, ζ(4p) = 1.15. For the $Au_{10}Cr_4Zn_{89}$ calculation, all sites used these parameters, and site preferences were determined by Mulliken population analysis.[35] There were 28 k-points in the irreducible wedge, but 108

dx.doi.org/10.1021/ic302244e | Inorg. Chem. 2013, 52, 4812−4818

k-points were used to make sure all symmetry-equivalent bonds were included for the population analysis.

RESULTS AND DISCUSSION

Phase Analysis. The homogeneity range of cubic γ-brass phases in the Au−Cr−Zn system was examined by means of preparative methods, calorimetric measurements, X-ray diffraction, and EDS analyses.

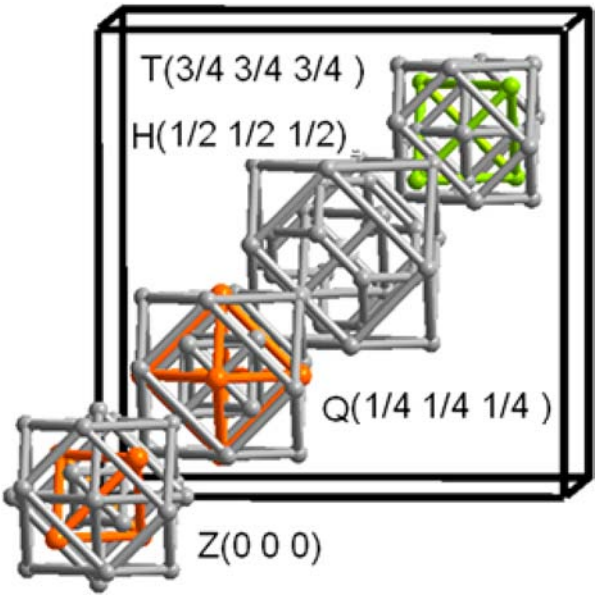

Figure 2. Arrangement of clusters in the crystal structure of $Au_{10}Cr_4Zn_{89}$ along the body diagonal. The clusters are centered about the high symmetry points of the *F*-centered cubic unit cell. The clusters are represented by idealized cuboctahedral shells. Zinc atoms are shown in gray, chromium in lime, and gold in orange.

Chemical compositions determined by EDS and X-ray single crystal refinement agree well and show an extended homogeneity range over $0.026 \leq x_{Au} \leq 0.097$ and $0.063 \leq x_{Cr} \leq 0.039$, that is, from $Au_{2.6}Cr_{6.4}Zn_{91.7}$ to $Au_{10.0}Cr_{4.0}Zn_{89.0}$. The sample with nominal composition $Au_{10.0}Cr_{4.0}Zn_{89.0}$ coexists with a competing binary phase of approximate composition $AuZn_7$[36] (ε-phase, space group $P6_3/mmc$, prototype Mg) as observed by EDX analysis and X-ray powder diffraction experiments. Specimens with $x_{Au} \leq 0.026$ form randomly oriented, multiply twinned crystals that do not allow high quality structural refinements. The melting point of the target phase increases with increasing gold content. Recrystallization does not occur at the chosen cooling rate of 10 K h^{-1}, and the phase does not reform even after 12 h annealing.

Structural Characteristics. The ternary phase in the Au−Cr−Zn system crystallizes in the acentric space group $F\bar{4}3m$ with approximately 402−412 atoms in the cubic unit cell that are distributed over 15−20 crystallographically independent positions depending on the chemical composition of the phase.

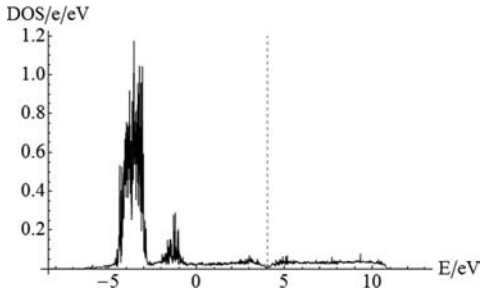

Figure 3. Total density of states of $Au_{10}Cr_4Zn_{89}$. The first two large peaks are due to the Zn and Au d-orbitals respectively. Also note the pseudogap formation at the Fermi energy. The vertical axis is given in units of states per valence electron so that the DOS plot is comparable between systems with different sized unit cells.

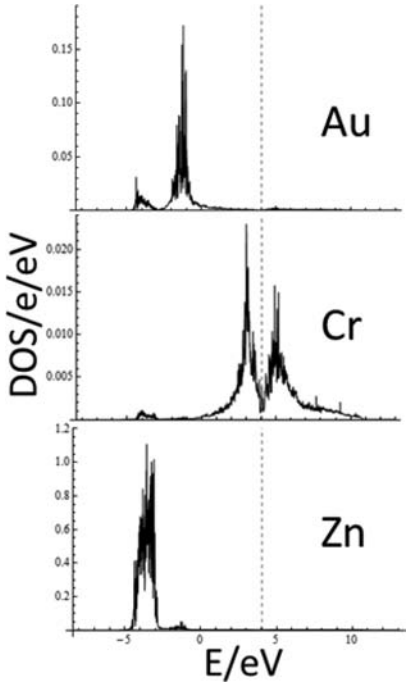

Figure 4. Partial DOS of projected d-states for (from top to bottom) Au, Cr, and Zn, respectively. All plots are truncated vertically so that we can see the structure near the Fermi level. The Cr plot (middle) clearly shows the d-states are split at the Fermi level. Note the difference in scale reflecting the relative quantities of Au, Cr, and Zn.

The structure of the phases adopts a $6 \times 6 \times 6$ superstructure of a body centered cubic type structure with ordered vacancies,[37] or, alternatively, $2 \times 2 \times 2$ superstructure of a γ-brass related structure.[38]

The binary phase $CrZn_{17}$ is disordered exhibiting a complex interplay of occupational and displacive disorder, but this disorder decreases upon substitution of Cr and Zn for Au, and at the limiting composition $Au_{10}Cr_4Zn_{89}$ the structure is fully ordered (Figure 2). It is therefore convenient to describe the

Table 1. Decoration of the Four Clusters in $Au_{10}Cr_4Zn_{89}$

cluster	CC(1)	IT(4)	OT(4)	OH(6)	TT(12)	CO(12)	cluster type
Z (0 0 0)		Zn11	Au12	Zn13		Zn15	γ-type $Zn_{22}Au_4$
Q ($^1/_4$ $^1/_4$ $^1/_4$)		Zn21	Zn22	Au23		Zn25	γ-type $Zn_{20}Au_6$
H ($^1/_2$ $^1/_2$ $^1/_2$)	Zn30		Zn32		Zn34	Zn35	α-Mn type Zn_{29}
T ($^3/_4$ $^3/_4$ $^3/_4$)			Cr42	Zn43		Zn45	Ti_2Ni type $Zn_{18}Cr_4$

dx.doi.org/10.1021/ic302244e | *Inorg. Chem.* 2013, 52, 4812−4818

Table 2. Relative Charges of Sites in Model All-Zn System Corresponding to Experimental Sites

site	charge
Au23 (QOH)	−0.14
Au12 (ZOT)	−0.13
Zn32 (HOT)	−0.06
Zn21 (QIT)	−0.03
Zn22 (QOT)	−0.02
Zn25 (QCO)	−0.01
Cr42 (TOT)	0.00
Zn15 (ZCO)	0.00
Zn34 (HTT)	0.02
Zn13 (ZOH)	0.03
Zn45 (TCO)	0.03
Zn35 (HCO)	0.05
Zn11 (ZIT)	0.06
Zn30 (HCC)	0.06
Zn43 (TOH)	0.06

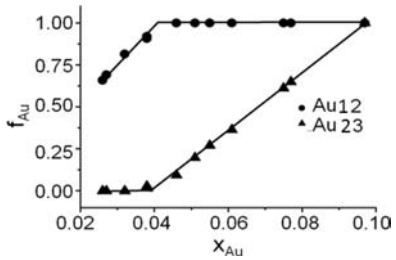

Figure 5. Representation of substitutional disorder: SOF of gold (f_{Au}) (at OT site of cluster Z and perfect octahedral site of cluster Q) vs mole fraction of Au (x_{Au}) in the Au−Cr−Zn system.

structure with this ordered ternary compound as the archetype and the less ordered, Au poor, ternaries as well as the Cr−Zn binary as derivatives thereof.

$Au_{10}Cr_4Zn_{89}$ may be regarded as arrangements of nested polyhedral units,[39,40] isolated or linked, centered at sites of high symmetry points. Such arrangements of nested polyhedral unit have been termed "clusters",[41] but this is a purely geometric description. These aggregates of atoms are not actually clusters in a chemical sense, and they are not separated from the rest of the structure. They constitute sets of atoms that simplify the task of visualizing complicated structures.

The four constitutive clusters are located at the high symmetry points of the unit cell, and designated by capital letters indicating their respective position: Z:(0 0 0); Q:($^1/_4$ $^1/_4$ $^1/_4$); H:($^1/_2$ $^1/_2$ $^1/_2$), and T:($^3/_4$ $^3/_4$ $^3/_4$).[42] Furthermore, within each cluster the atomic shells are distinguished by two capital letters in congruence with the standard used for γ-brass clusters. CC designates the center of a cluster, IT those occupying the vertices of an inner tetrahedron, OT stands for outer tetrahedron, OH is an octahedral shell, TT for truncated tetrahedron, and CO for cuboctahedron. These shells are never all simultaneously occupied. The decoration of the four clusters in $Au_{10}Cr_4Zn_{89}$ is shown in Table 1.

Electronic Structure Calculation. The site preferences of $Au_{10}Cr_4Zn_{89}$ are puzzling. In particular, why should two neighboring γ-brass clusters color different sites with Au: one on the inner tetrahedron site, and the next on the octahedron site (Figure 2). As mentioned in the introduction, the Hume−Rothery rules are heuristic guidelines for rationalizing the structure of metal compounds at particular electron counts.[43] A wide variety of intermetallic structures seem to form according to this principle, including compounds of alkali and alkaline earth metals, transition metals, noble metals, and metalloids.[44] Recurring structural motifs include fragments from the structures of γ-brass, α-Mn, Ti_2Ni, and bcc.[45] An extended structure is a Hume−Rothery structure if (1) its electronic structure depends primarily on s- and p- orbital interactions and (2) the s- and p- electron count is near that of Cu_5Zn_8 (21/13 ≈ 1.62 e/a). This means that d-orbitals of the constituent atomic sites are filled and for the most part not involved in bonding.

A straightforward approach is simply to fill the d-orbitals completely. The valence d-shells of Au and Zn are already full: $5d^{10}6s^1$ and $3d^{10}4s^2$, respectively. Hence, Au contributes 1 electron, and Zn contributes 2. Cr has a half-filled d-shell, $3d^54s^1$. Therefore, to fill its d-shell, Cr contributes −4 electrons. This counting scheme gives 1.67 e/a, which is very close to the Hume−Rothery γ-brass standard.

Is that a reasonable assumption for $Au_{10}Cr_4Zn_{89}$? To find out, we used DFT-LDA (see Computational Details section). In particular, we look at the projected d-states, with caveats. The total DOS is encouraging: there appear to be localized, filled d-orbitals well below the Fermi energy, as well as good pseudogap formation (Figure 3). To test whether the d-orbital states are filled, we investigated the projected d-DOS for each atom type: Au, Cr, and Zn. Since VASP uses a plane-wave basis set rather than atomic orbital basis set, the projections are not perfect. In particular, adding together several projected DOS will typically not give the total DOS.

We can see in Figure 4 that for Au and Zn, the d-orbital density lies mostly below the Fermi level. Perfectly filled d-

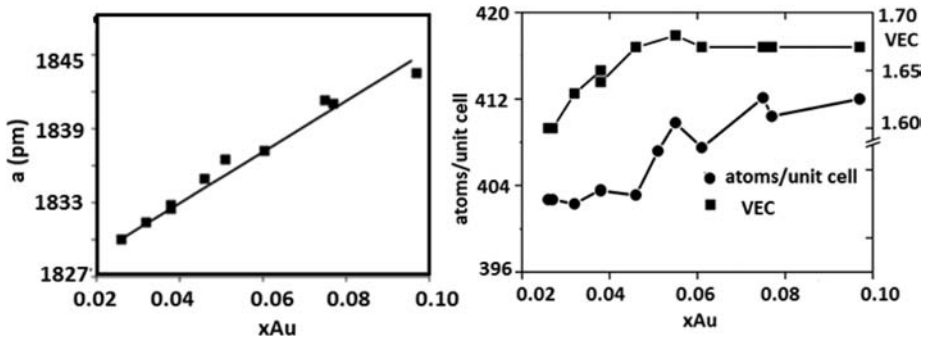

Figure 6. (Left) Variation of lattice parameters (a/pm) vs mole fraction of Au (x_{Au}) from powder X-ray diffraction experiment of Au−Cr−Zn phase. (Right) The *vec* values and the total number of atoms per unit cell calculated from the refined composition vs relative amount of gold (x_{Au}).

dx.doi.org/10.1021/ic302244e | *Inorg. Chem.* 2013, 52, 4812−4818

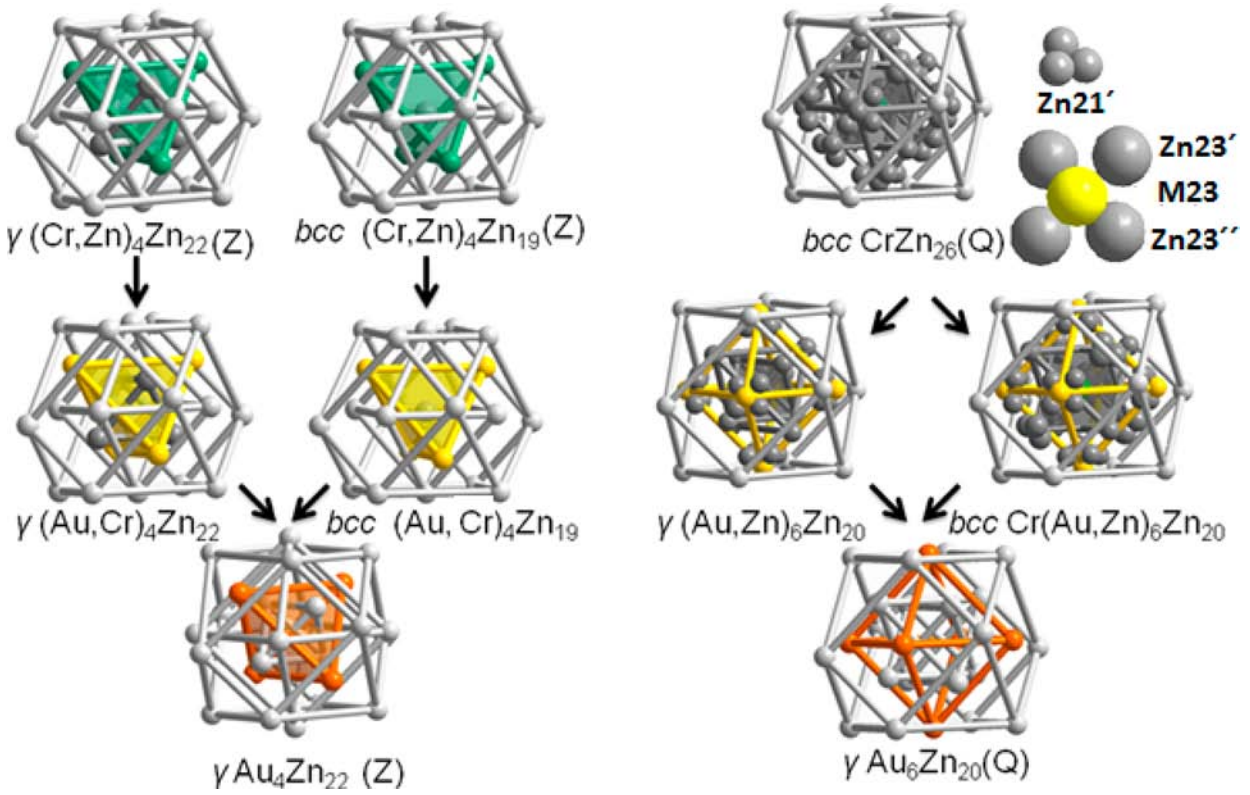

Figure 7. (left) Transmutation of cluster Z at (0 0 0) forms a mixture of defect bcc and γ-brass in the crystal structure of $Cr_{1.36}Zn_{23.79}$ to clean γ-type Au_4Zn_{22} in $Au_{10}Cr_4Zn_{89}$ by the progressive replacement of Cr and Zn by Au. Constituting zinc atoms have been shown in gray, Cr/Zn in sea green, and Au/Cr in gold and gold in orange, (right) Transmutation of cluster Q at $^1/_4$ $^1/_4$ $^1/_4$ from a bcc-type cluster to a clean γ-brass-type cluster by replacement of Cr and Zn by Au. Constituting zinc atoms have been depicted in gray, Au/Zn in gold, and Au in orange.

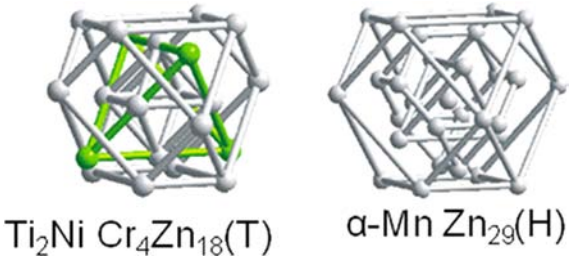

Figure 8. Representation of the cluster H at $^1/_2$ $^1/_2$ $^1/_2$ α-Mn-type Zn_{29} (right) and cluster T centered at $^3/_4$ $^3/_4$ $^3/_4$ $TiNi_2$-type Cr_4Zn_{18} (left)-unaffected by Au/Cr and/or Au/Zn replacement.

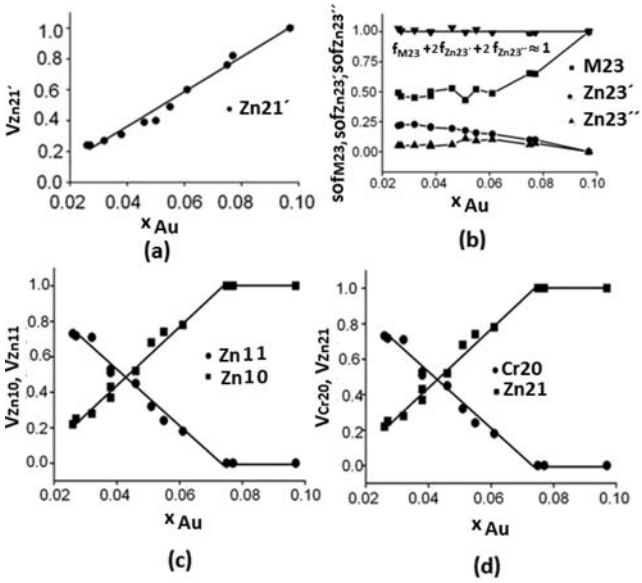

Figure 9. Representation of (a) random vacancy at the Zn21′ site ($V_{Zn21'}$ = 1−3 $SOF_{zn21'}$) versus relative amount of gold (x_{Au}), (b) positional disorder at OH, OH′, and OH″ sites of cluster Q: SOF_{M23}, $SOF_{Zn23'}$, $SOF_{Zn23''}$ vs mole fraction of Au (x_{Au}), (c) vacancy at Zn10 site (V_{Zn10} = 1 − SOF_{Zn10}) and Zn11 site (V_{Zn11} = 1 − SOF_{Zn11}) of cluster Z and (d) vacancy at Cr20 site (V_{Cr20} = 1 − SOF_{Cr20}) and at Zn21 site (V_{Zn21} = 1 − SOF_{Zn21}) of cluster Q vs mole fraction of gold (x_{Au}) in the Au−Cr−Zn system.

orbitals would result in 10 d-electrons per atom. Numerical integration over partial Au-d and Zn-d states up to the Fermi level gives 8.7 and 10.0 electrons in d-states per atom, respectively.

Contrast Au and Zn to the Cr case. The projected Cr d-states are clearly split at the Fermi level and appear to be about half-filled, favoring a high spin configuration. In fact, integration gives 4.5 d-electrons per Cr. The half-filling suggests we take the Cr valence electron configuration as in the free atom: $3d^5 4s^1$. Then Cr contributes +1 e instead of −4 e, and the s- and p-electron count becomes 1.86 e/a, a significant deviation from the Hume−Rothery standard but comparable to some hcp compounds of noble metals.[44]

With a feasible electron-counting scheme in hand, we can focus on the question of site preferences. Here we turn to the extended Hückel (eH) method (see Computational Details). In particular, we will use Mulliken population analysis to tell us the electron population on different sites. If there is a chemical rationale behind the site coloring, eH should capture it. Our

dx.doi.org/10.1021/ic302244e | Inorg. Chem. 2013, 52, 4812−4818

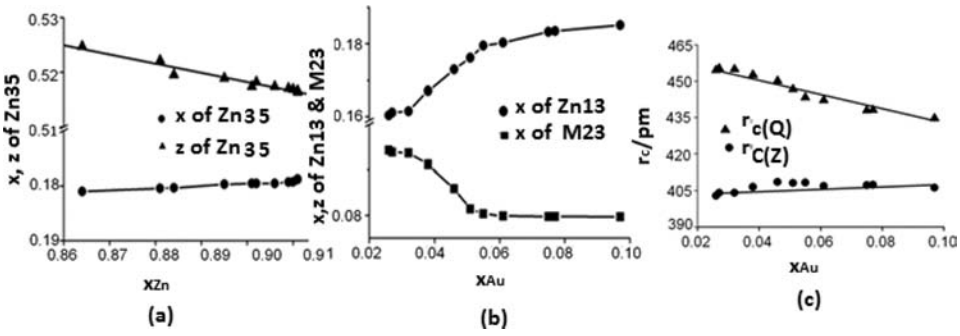

Figure 10. (a) Positional parameters (x, z) for Zn35 site of cluster H vs mole fraction of Zn (x_{Zn}), (b) positional parameters (x) for Zn13 and M23 sites vs mole fraction of Au (x_{Au}), and (c) effective cluster dimensions ($r_{C(Z)}$, $r_{C(Q)}$) for cluster Z and Q vs mole fraction of Au (x_{Au}) from single crystal X-ray diffraction experiment of the various Au−Cr−Zn specimens.

strategy is to model all sites as the majority element, Zn, and see which sites accumulate the most electrons. The most electron-rich sites should correspond to the most electronegative element, Au (Pauling electronegativity 2.54 versus 1.66 for Cr and 1.65 for Zn[46]). This approach has been used reliably for intermetallic structures in the past.[34,47,48]

Our analysis agrees very well with the experimentally found sites (Table 2), particularly in distinguishing the Au sites from the remaining Zn and Cr sites. That we were unable to distinguish the Cr site from the Zn sites is not surprising given that Cr and Zn are similar in electronegativity and the extent to which the Cr d-orbitals play a role in bonding is not taken into account.

Exchange Mechanisms. Taking the fully ordered ternary phase as a reference, the structures of the compounds with a lower gold content can now be understood in terms of a sequence of exchange mechanisms. The clusters H and T are invariant with respect to the exchange of Au for Cr and Zn and not only do their compositions remain Zn_{29} and Cr_4Zn_{18} throughout the homogeneity range of ternary phase, but the positional parameters also remain unchanged to within 3 pm.

The variable part of the structure consists of the Z and the Q clusters. It varies in composition between $Au_{2.64}Cr_{2.36}Zn_{44.72}$ and $Au_{10.0}Zn_{42.0}$. The variation of composition is accompanied by various disorder phenomena. The depletion of Au follows a simple and clear pattern. When the amount of Au is decreased, the occupancy of Au23 decreases linearly to zero. Only after this position is empty does the occupancy of the second Au position, Au12 start to decrease (Figure 5).

The local rearrangements in the clusters involved, Z and Q, are more complex. This is due to both the Hume−Rothery rules and volumetric constraints (Figure 6) (Gold is considerably larger than either Zn or Cr, (atomic volumes: Au 10.2 cm^3 mol^{-1}, Cr 7.23 cm^3 mol^{-1}, Zn 9.2 cm^3 mol^{-1})).

Cluster Z transmutes from a mixture of a defect bcc- and γ-brass-type clusters to a clean γ-brass type Au_4Zn_{22} cluster (Figure 7 left) by the progressive replacement of Cr and/or Zn by Au, and cluster Q transforms from a β-brass-type cluster to a clean γ-brass type Au_6Zn_{20} over the mixture of β- and γ-brass types by Au/Cr and/or Au/Zn replacement (Figure 7 right). Clusters H and T are compositionally ordered and remain unaffected by Cr and Zn replacement by Au throughout the whole homogeneity range of the phase (Figure 8). Hence, in the phase richest in Au all kinds of disorders have vanished (Figure 9) in favor of the formation of perfectly ordered Au_4Zn_{22} and Au_6Zn_{20} γ-brass-type clusters.

With increasing zinc content, x values of Zn35 site increase linearly whereas z values drop (Figure 10a), though the H cluster remains compositionally intact throughout the homogeneity range by Cr/Au and/or Zn/Au replacement. Furthermore, x values associated with Zn13 in cluster Z increase and the x values of M23 in cluster Q decrease parallel to Au insertion in the phase (Figure 10-b).

The effective cluster dimension, (i.e., circumference radii r_C for respective cuboctahedra, given by the distance between their center (CC site) and their vertices (CO site)) of the compositionally conserved clusters (H, T) endures marginal variation. On the other hand, cluster Q shows a notable variation in its effective dimension, whereas cluster Z does not change significantly in size, though both Q and Z form the compositionally variable partial structure. (Figure 10c). Moreover, the γ-brass cluster of composition Au_6Zn_{20} ($r_{C(Q)}$ = 435 pm) evolves a volume approximately 20% larger than that of the congeneric Au_4Zn_{22} cluster ($r_{C(Q)}$ = 406 pm).

CONCLUSION

A systematic investigation of chemical substitution of Au into the Cr−Zn system has uncovered a $(2a_\gamma)^3$ superstructure of γ-brass related phase ranging from $Au_{2.6}Cr_{6.4}Zn_{91.7}$ to $Au_{10.0}Cr_{4.0}Zn_{89.0}$. According to the single crystal diffraction experiments, the ternary phase crystallizes in the acentric space group $F\bar{4}3m$ with approximately 403−412 atoms in the cubic unit cell, having a significant phase width. The structure of the cubic phase consists of six distinctive clusters each having 22−29 atoms arranged at 16 high symmetry points of the unit cell. The structure can be divided into two partial structures, and the centers of each cluster of two partial structures form two interpenetrating zinc blende like nets. One partial structure consists of clean α-Mn-type Zn_{29} (H) and $NiTi_2$-type Cr_4Zn_{18} (T) clusters and remains unaffected by the replacement of Cr and/or Zn by Au over the homogeneity range. Its complement shows variable composition and hosts three types of disorders such as vacancies (Zn10/Zn11, Cr20/Zn21, Zn21′), substitutional (Au and Cr or Au and Zn), and positional disorder (M23/Zn23′/Zn23″ and Zn21′) in the form of split positions. Over the composition range disordered γ-brass type and defect bcc type clusters transmute to clean γ-brass type Au_4Zn_{22} and disordered bcc type clusters transform to clean γ-brass type Au_6Zn_{20} via an intermediate mixture of bcc and γ-brass type clusters.

An extensive study of compositionally different crystals in the Au−Cr−Zn system reveals a systematic spatial correlation among the SOFs of vacancy sites, mixed occupied and

dx.doi.org/10.1021/ic302244e | Inorg. Chem. 2013, 52, 4812−4818

positional disordered sites. The dependence of various kinds of disorders is controlled by valence electron concentration in the context of Hume−Rothery type stabilization. The valence electron concentration per atom ranges from 1.60 to 1.68—very close to the 21/13 expected value from the Hume−Rothery rule in gold poor structures.

Note: The structure solution and the refinement of the structure of $Au_{2.10}Cr_{6.9}Zn_{91.31}$ were carried out using the JANA2006 program (see Supporting information).[49,50]

■ ASSOCIATED CONTENT

Ⓢ Supporting Information

X-ray crystallographic files in CIF file format. Further details are given in Figures S1−S3 and Tables S1−S53. This material is available free of charge via the Internet at http://pubs.acs.org. Crystallographic data for compounds has been deposited with the Cambridge Crystallographic Data Centre under CCDC 903032−903047.

■ AUTHOR INFORMATION

Corresponding Author

*Fax: +46462224012. Tel: +46462224769. E-mail: Partha.Jana@polymat.lth.se.

Notes

The authors declare no competing financial interest.

■ ACKNOWLEDGMENTS

The authors wish to thank the Deutsche Forschungsgemeinschaft (DFG) and VR, the Swedish National Science Reasearch Council for the financial support. The authors would like to thank especially to Prof. Roald Hoffmann for many useful comments.

■ REFERENCES

(1) Hume-Rothery, W. *J. Inst. Met.* **1926**, *35*, 309.
(2) Hume-Rothery, W.; Raynor, G. V. *The Structure of Metals and Alloys*; Institute of Metals: London, U.K., 1954.
(3) Pearson, W. B. *The Crystal Chemistry and Physics of Metals and Alloys*; Wiley-Interscience: New York, 1972, pp 80−133.
(4) Pettifor, D. G. *Bonding and Structure of Molecules and Solids*; Oxford Science Publications: Oxford, U.K., 1995.
(5) Brandon, J. K.; Brizard, R. Y.; Chieh, P. C.; McMillan, R. K.; Pearson, W. B. *Acta Crystallogr. Sect. B* **1974**, *30*, 1412−1417.
(6) Heidenstam, Olov, v.; Johansson, A.; Westman, S. *Acta Chem. Scand.* **1968**, *22*, 653−661.
(7) Gourdon, O.; Gout, D. J.; Williams, J.; Proffen, T.; Hobbs, S.; Miller, G. J. *Inorg. Chem.* **2007**, *46*, 251−260.
(8) Johansson, A.; Ljung, H.; Westman, S. *Acta Chem. Scand.* **1968**, *22*, 2743−2753.
(9) Gross, N.; Kotzyba, G.; Kunnen, B.; Jeitschko, W. *Z. Anorg. Allg. Chem.* **2001**, *627*, 155−163.
(10) Arnberg, L.; Westman, S. *Acta Chem. Scand.* **1972**, *26*, 513−517.
(11) Gourdon, O.; Miller, G. J. *Chem. Mater.* **2006**, *18*, 1848−1856.
(12) Gourdon, O.; Izaola, Z.; Elcoro, L.; Petricek, V.; Miller, G. J. *Philos. Mag.* **2006**, *86*, 419−425.
(13) Jana, P. P.; Lidin, S. *Inorg. Chem.* **2012**, *51*, 9893−9901.
(14) Morton, A. J. *Phys. Status Solidi A* **1974**, *23*, 275−289.
(15) Thimmaiah, S.; Conrad, M.; Lee, S.; Harbrecht, B. *Z. Anorg. Allg. Chem.* **2004**, *630*, 1762.
(16) Mahne, S.; Harbrecht, B. *J. Alloys Compd.* **1994**, *203*, 271−279.
(17) Jana, P. P.; Lidin, S. *CrystEngComm* **2013**, *15*, 745−753.
(18) Koster, A. S.; Schoone, J. C. *Acta Crystallogr., Sect. B* **1981**, *37*, 1905−1907.
(19) Nasch, T.; Jeitschko, W. *J. Solid State Chem.* **1999**, *143*, 95−103.
(20) Thimmaiah, S.; Richter, K. W.; Lee, S.; Harbrecht, B. *Solid State Sci.* **2003**, *5*, 1309−1317.
(21) Hornfeck, W.; Thimmaiah, S.; Lee, S.; Harbrecht, B. *Chem.—Eur. J.* **2004**, *10*, 4616−4626.
(22) Jana, P. P. Dissertation, University of Marburg, Marburg, Germany, 2011.
(23) *IPDS, Program Package for X-ray Diffraction*, Version 2.75; Stoe & Cie.: Darmstadt, Germany, 1996.
(24) *X-RED −Data Reduction Program*, Version 1.02; Stoe & Cie.: Darmstadt, Germany, 2001.
(25) *X-SHAPE, Crystal Optimization for Numerical Absorption Correction*, Version 2.01; Stoe & Cie.: Darmstadt, Germany, 2001.
(26) Sheldrick, G. M. *SHELX-97, A Program Package for the Solution and Refinement of Crystal Structures*; Universität Göttingen: Göttingen, Germany, 1997.
(27) Kresse, G.; Hafner, J. *J. Phys. Rev. B* **1993**, *47*, 558−561.
(28) Kresse, G.; Hafner, J. *Phys. Rev. B* **1994**, *49*, 14251−14269.
(29) Kresse, G.; Furthmüller, J. *Comput. Mater. Sci.* **1996**, *6*, 15−60.
(30) Kresse, G.; Furthmüller, J. *Phys. Rev. B* **1996**, *54*, 11169−11186.
(31) Perdew, J. P.; Zunger, A. *Phys. Rev. B* **1981**, *23*, 5048−5079.
(32) Vanderbilt, D. *Phys. Rev. B* **1990**, *41*, 7892−7895.
(33) Kresse, G.; Hafner, J. *J. Phys.: Condens. Matter* **1994**, *6*, 8245−8257.
(34) Gaston, N.; Paulus, B.; Wedig, U.; Jansen, M. *Phys. Rev. Lett.* **2008**, *100*, 226404.
(35) Hoffmann. R. *Solids and Surfaces: A Chemist's View on Bonding in Extended Structures*; VCH Publishers, Inc.: New York, 1988.
(36) Massalski, T. B.; King, W. H. *Acta Metall.* **1962**, *10*, 1171−1181.
(37) Nesper, R.; Von Schnering, H. G. *J. Solid State Chem.* **1987**, *70*, 48−57.
(38) Bradley, A. J.; Thewlis, J. *Proc. Roy. Soc. London A* **1926**, *112*, 678−692.
(39) Chabot, B.; Cenzual, K.; Parthe, E. *Acta Crystallogr., Sect. A* **1981**, *37*, 6−11.
(40) Hellner, E.; Koch, E. *Acta Crystallogr., Sect. A* **1981**, *37*, 1−6.
(41) Nowotny, H.; Bauer, E.; Stempfl, A. *Monatsh. Chem.* **1950**, *81*, 679−680.
(42) Berger, R. F.; Lee, S.; Johnson, J.; Nebgen, B.; So, A. C. Y. *Chem.—Eur. J.* **2008**, *14*, 6627−6639.
(43) Hume-Rothery, W.; Smallman, R. W.; Haworth, C. W. *The Structure of Metals and Alloys*; The Institute of Metals: London, U.K., 1969.
(44) Hoistad, L. M.; Lee, S. *J. Am. Chem. Soc.* **1991**, *113*, 8216−8220.
(45) Dshemuchadse, J.; Jung, D. Y.; Steurer, W. *Acta Crystallogr., Sect. B* **2011**, *67*, 269−292.
(46) Pauling, L. *The Nature of the Chemical Bond*, 3rd ed.; Cornell University: Ithaca, NY, 1960.
(47) Schmidt, J.; Lee, S.; Fredrickson, D.; Conrad, M.; Sun, J.; Harbrecht, B. *Chem.—Eur. J.* **2007**, *13*, 1394−1410.
(48) Berger, R.; Lee, S.; Hoffmann, R. *Chem.—Eur. J.* **2007**, *13*, 7852−7863.
(49) Petricek, V.; Dusek, M.; Palatinus, L. *The Crystallographic Computing System, Jana 2006*; Institute of Physics: Praha, Czech Republic, 2006.
(50) Palatinus, L.; Chapuis, G. *J. Appl. Crystallogr.* **2007**, *40*, 786−790.